Chapter 4: Binocular combination in the Autonomic Nervous System

Federico G. Segala[1], Joel T. Martin[1], Alex R. Wade[1, 2] & Daniel H. Baker[1, 2]

[1]Department of Psychology, University of York, York, UK. YO10 5DD
[2]York Biomedical Research Institute, University of York, York, United Kingdom

Address for correspondence: Federico G. Segala, federico.segala@york.ac.uk

1 Abstract

The size of the pupils changes in response to levels of ambient light and is regulated by the autonomic nervous system. The role of the retinal photoreceptors in determining pupil size has been investigated using silent substitution. They have been shown to be directly involved in controlling and maintaining the size of the pupils, with the cones and rods driving the initial constriction and the intrinsically photosensitive retinal ganglion cells maintaining the size over prolonged time periods. Here, we used silent substitution and pupillometry to investigate binocular combination while targeting the intrinsically-photoreceptive retinal ganglion cells, the L-M pathway and the S-(L+M) pathway. We found that the signals between the two pupils are combined in a non-linear manner when targeting all the different photoreceptor classes and that the non-linear combination was different between each class, as reflected by the different magnitudes of interocular suppression measured for each pathway.

2 Introduction

The autonomic nervous system regulates many involuntary bodily processes, including the constriction and dilation of the pupils in response to light (McDougal and Gamlin, 2015). The anatomical pathway from the retina to the subcortical nuclei controlling the pupillary light response (PLR) is well established: it includes the Pretectal Olivary nucleus (PON), the Superior Cervical ganglion and the Edinger-Westphal nucleus, which project to the iris sphincter muscles that directly control the pupil size (McDougal and Gamlin, 2015, 2008; Wang and Munoz, 2015). Additionally, the retinal photoreceptors (cones, rods and the recently discovered melanopsin-containing intrinsically photosensitive retinal ganglion cells, ipRGCs) have been shown to be directly involved in controlling and maintaining the size of the pupils (Barrionuevo et al., 2018, 2014; Dacey et al., 2005; Murray et al., 2018; Spitschan, 2019; Spitschan et al., 2014; Woelders et al., 2018). The cones have been shown to drive the initial rapid constriction of the pupils (Mathôt, 2018), while the slower and longer activation of the ipRGCs shows their role in maintaining the constriction over a prolonged period of time and in regulating the post-illumination pupillary response (Markwell et al., 2010; McDougal and Gamlin, 2010).

The ipRGCs are a unique photoreceptor class that has been discovered recently (Provencio et al., 2000). They express the photopigment melanopsin, which is involved in the regulation of the circadian rhythm (Panda et al., 2002; Provencio et al., 2000; Ruby et al., 2002), and form a major input to the PON (Dacey et al., 2003). The first direct evidence of the involvement of the ipRGCs in the PLR was shown in rats by Lucas et al. (2003) who genetically deleted the melanopsin gene from rats, resulting in the loss of the intrinsic photosensitivity of the cells and a reduced pupil constriction. This same behaviour was later also

observed in primates and humans (Gamlin et al., 2007), where it was demonstrated that the PLR continues during light presentation even when cone and rod signalling is blocked. This also demonstrates the primary role of the ipRGCs in maintaining pupil constriction over a prolonged time. It has also been shown that the ipRGCs receive inputs from the other photoreceptors (cones and rods) and are activated by them (Dacey et al., 2005).

To investigate how specific photoreceptor classes control the size of the pupils, a technique known as silent substitution is used. Silent substitution exploits the fact that each photoreceptor class has a distinct spectral tuning that overlaps with the others. Using a multiprimary system, in which the primaries have different spectra, it is possible to target one class of photoreceptors while maintaining the others at a constant activity level, effectively silencing them (Shapiro et al., 1996; Spitschan and Woelders, 2018, this paper also offers a clear explanation of how to implement silent substitution). Studies using silent substitution have shown that the pupils behave differently depending on which photoreceptor or pathway is being stimulated. For example, pupil responses have been shown to be out of phase when the S cones are stimulated, relative to when the ipRGCs or the L+M cones are stimulated (Cao et al., 2015; Spitschan et al., 2014). Additionally, when L and M cones are stimulated individually, there appears to be a paradoxical pupil response: increments in L cone stimulation cause a constriction of the pupil, while increments in M cone stimulation lead to a dilation of the pupil (Murray et al., 2018; Woelders et al., 2018).

Interaction between the two eyes and the rules of binocular combination have been extensively studied. For pattern vision in the visual cortex, at low contrast, binocular summation occurs (binocular presentation confers higher sensitivity than monocular presentation, Baker et al., 2018; Campbell and Green, 1965; Legge, 1984), while, at high contrast, ocularity invariance is implemented (the response to monocularly- and binocularly-presented patterns is equalised, Baker et al., 2007; Ding and Sperling, 2006; Meese et al., 2006). Additionally, evidence of a binocular component to the PLR is shown by the existence of a consensual response of the pupil (the stimulation of one eye will cause constriction of the other eye, Wyatt and Musselman, 1981) and the rules of binocular combination between the pupils have also been recently investigated (Segala et al., 2023), finding that combination happens non-linearly with evidence of interocular suppression.

Most of the studies that use silent substitution and that investigate the PLR stimulate only one eye. If the stimulated eye is pharmacologically dilated to control pupil size, the response from the unstimulated eye (known as the consensual response) can be recorded (e.g. McDougal and Gamlin, 2010; Spitschan et al., 2014). While this approach controls the total amount of light incident at the retina, it does not permit investigation of binocular combination for specific photoreceptor pathways. Seeing that it is possible to directly investigate binocular combination of signals between the pupils, we decided to investigate this by designing an experiment that allowed us to binocularly target the ipRGCs, the L-M pathway and the S-(L+M) pathway individually while recording binocular pupillometric measures. We chose a primary flicker frequency of 0.5 Hz, which has been shown to elicit pupil responses from all three pathways (Spitschan et al., 2014). The final results are interpreted using a hierarchical Bayesian computational model of binocular vision.

3 Methods

3.1 Participants

Twenty-four participants were recruited for each of the four experiments for a total of ninety-six (68 females) adult participants, whose age ranged from 18 to 41. All participants had normal or corrected to normal binocular vision and normal colour vision, and gave written informed consent. Our procedures were approved by the Ethics Committee of the Department of Psychology at the University of York (identification number 184).

3.2 Apparatus & stimuli

To present synchronised silent substitution contrast modulations independently to each eye, two light engines, each with 10 independently addressable LED colour channels (SpectraTuneLAB: LEDMOTIVE Technologies, LLC, Barcelona, Spain), were integrated into a customised viewing system. The light engines were operated via a Python interface to their REST API (Martin et al., 2022), which supports synchronous launch and playback of spectral sequences prepared in advance and stored in JSON format. When preparing the spectral sequences, the age of participants was recorded to account for the yellowing of the lenses.

The output from the light engines was directed through liquid light guides (LLG3-8H: Thorlabs Ltd, Cambridgeshire, UK) and diffused onto semi-opaque and highly diffusive white glass discs with a diameter of 50 mm for even illumination (34-473: Edmund Optics, York, UK). The light guide gaskets were butt-coupled to the light engine diffusers with threaded adapters (SM1A9, AD3LLG: Thorlabs Ltd, Cambridgeshire, UK) and the exiting ends of the light guides were mated with 51 mm depth optical cylinders (SM2L20: Thorlabs Ltd, Cambridgeshire, UK) via appropriately threaded adapters (AD3LLG, SM2A6: Thorlabs Ltd, Cambridgeshire, UK). The stimulus diffuser discs were retained at the front end of the optical cylinders approximately 51 mm from the light source, at which distance the output beam was sufficiently dispersed to afford even illumination of the diffuser when viewed from the front. To guarantee safe illumination levels, a circular neutral-density filter with the same diameter of the white glass discs (50 mm) and an optical density of 0.6 log units was placed in the optical path between the light source and the diffusers. A small circular piece of blackout material with a diameter of approximately 8 degrees (10 mm) was positioned centrally on the front of each diffuser disc to aid as a fusion lock, as a fixation point and to occlude the fovea.

The diffuser discs were positioned in the objective planes of the lenses of a modified VR headset (SHINECON SC-G01, Dongguan Shinecon Industrial Co. Ltd), which was used by the participants to view the stimuli. The stimuli were two discs of flickering light with a diameter of approximately 30 degrees, which were fused together into a cyclopean percept resembling a donut-shaped ring of light, similar to that used in other studies (e.g., Barrionuevo and Cao, 2016; Murray et al., 2018; Spitschan et al., 2014; Zele et al., 2018). The VR headset modifications allowed for small adjustments to account for individual differences in interpupillary distance and focal length. The use of this set up allowed us to modulate the stimuli in three different ocular configurations, similar to the ones we used in our previous experiment (Segala et al., 2023): monocular, binocular and dichoptic. In the monocular configuration, the unstimulated eye still saw a non-flickering disc of mean luminance. A schematic of the stimulation system is shown in Figure 1a. Pupillometry data were collected using a binocular Pupil Core eye-tracker headset (Pupil Labs GmbH, Berlin, Germany, Kassner et al., 2014) running at 120 Hz, and the signals were recorded with the Pupil Capture software.

3.3 Procedure

Before the start of each experiment, participants adjusted the objective planes of the lenses with the help of the experimenter until the stimulus was in focus and they perceived the two pieces of blackout material as one fused piece.

We initially planned to examine pupil responses and EEG responses simultaneously to temporal modulations flickering at 2 Hz and 1.6 Hz while stimulating the periphery of the retina. While the experiment produced clear responses when presenting an achromatic light (see Figures **??** and **??** in Appendix 1), the responses were very noisy for the targeted photoreceptor class experiments (see Figures **??**-**??** in Appendix 2) for both the pupillometry and the EEG data. Therefore, we decided to lower the main frequency to 0.5 Hz as previous literature showed that it was slow enough to elicit a pupil response from all photoreceptor classes (Spitschan et al., 2014) and we focussed on only recording pupillometry data as this frequency would be well below the minimum threshold to elicit EEG responses (Norcia et al., 2015).

Pupil responses to binocular temporal contrast modulations were examined in a factorial design that combined six ocular conditions, two temporal frequencies (0.4 and 0.5 Hz) and five temporal contrast levels relative to the mean illuminance (6, 12, 24, 48 and 96%). This design, similar to what we used in our previous study (Segala et al., 2023), was applied in four separate experiments, each with a different mode of

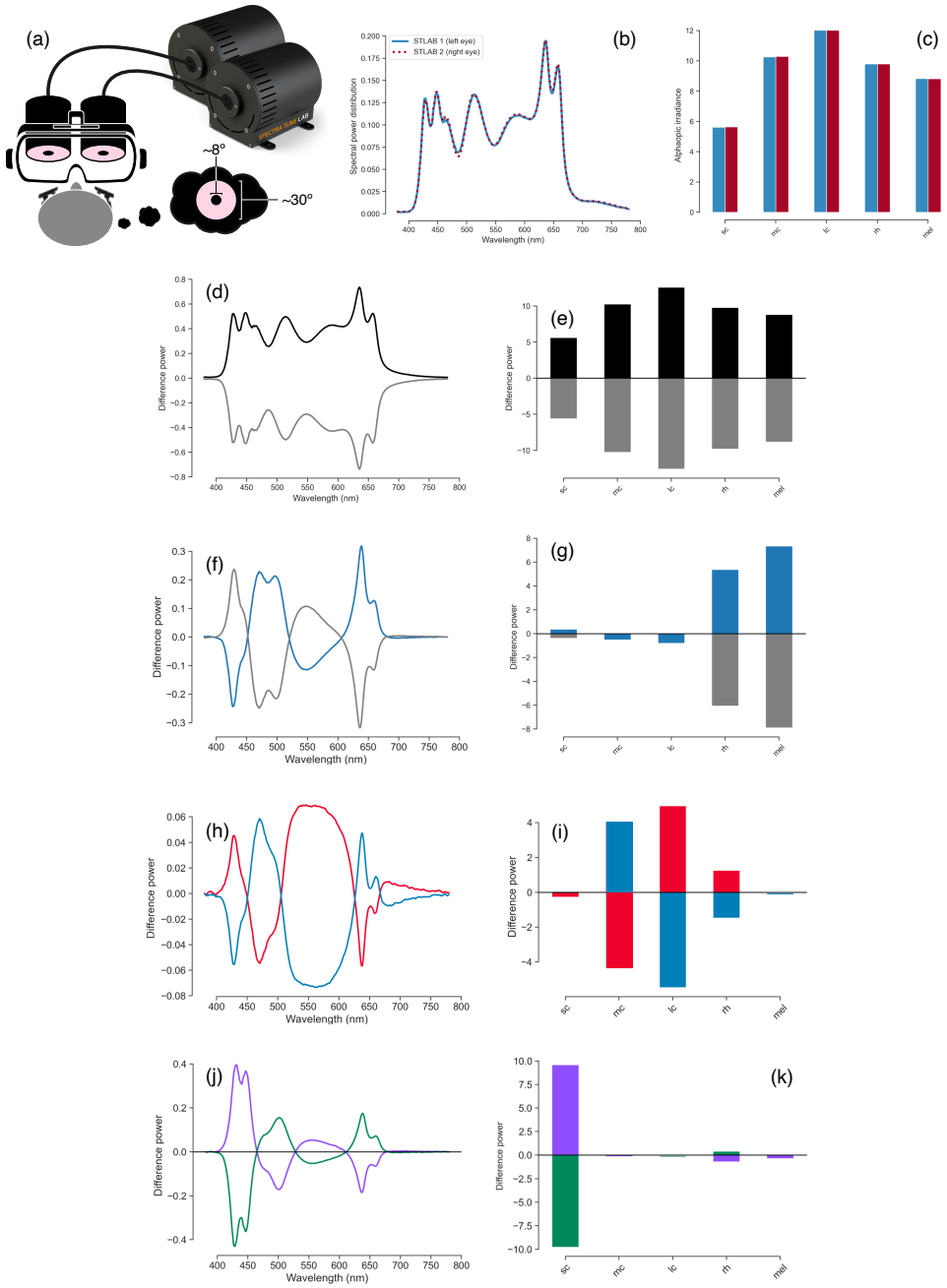

Figure 1: Summary of the spectral power distributions and alpha-opic irradiances for the background and each experiment. Panel (a) shows a schematic of the binocular stimulation system for presenting spectrally tuned modulations independently to each eye. The VR headset was attached to a clamp stand that the experimenters could use to adjust the height and align the headset with the eyes of the participant. The participant's head was positioned on a chin rest to keep it in position throughout the entire experiment. Panels (b) and (c) show the spectral power distributions and the alpha-opic irradiances of the background spectra used for both eyes. Panels (d-k) show the power distributions and the alpha-opic irradiances relative to the background for the four experiments: luminance (d, e), melanopsin (f, g), L-M pathway (h, i) and S-(L+M) pathway (j, k). A positive difference power shows a positive modulation (white disc for the luminance experiment, magenta for the L-M pathway experiment and purple for the S-(L+M) experiment) and a negative difference power shows a negative modulation (black disc for the luminance experiment, cyan for the L-M pathway experiment and lime for the S-(L+M) experiment).

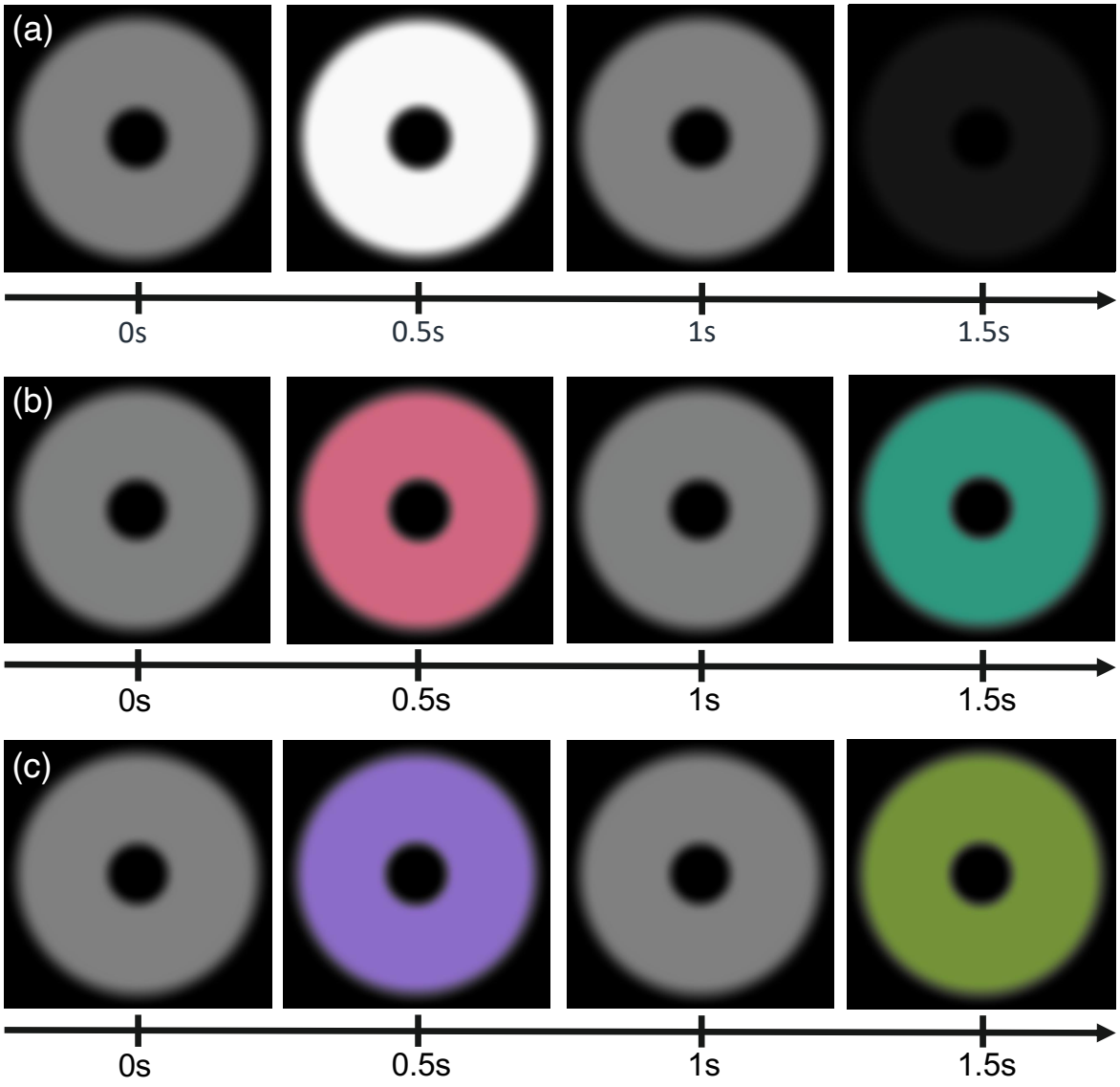

Figure 2: Example of the different experimental conditions. Panel (a) shows one cycle of flicker in the achromatic luminance experiment. In this experiment, the stimulus flickers between black and white. At the beginning of the cycle (0s), the stimulus appears at half the intesity and appears grey to the viewer. At 0.5s, the stimulus reaches the maximum intensity of the flicker and appears white to the viewer. At 1s, the stimulus appears again at half maximum and once again appears to be grey to the viewer. At 1.5s, the stimulus reaches the minimum intensity of the flicker and appears black to the viewer. Panel (b) shows one cycle of the flickering in the L-M pathway experiment. In this experiment, the stimulus flickers between magenta (+L-M) and cyan (-L+M). At the beginning of the cycle (0s), the stimulus appears at zero cone contrast and appears to be grey to the viewer. At 0.5s, the stimulus reaches the maximum L-cone contrast and appears magenta to the viewer. At 1s, the stimulus appears again at zero cone contrast and switches colour, once again appearing to be grey to the viewer. At 1.5s, the stimulus reaches the minimum L-cone contrast and appears cyan to the viewer. Panel (c) shows one cycle of the flickering in the S-(L+M) pathway experiment. In this experiment, the stimulus flickers between purple (+S-(L+M)) and lime (-S+(L+M)). At the beginning of the cycle (0s), the stimulus appears at zero cone contrast and appears to be grey to the viewer. At 0.5s, the stimulus reaches the maximum S-cone contrast and appears purple to the viewer. At 1s, the stimulus appears again at zero cone contrast and switches colour, once again appearing to be grey to the viewer. At 1.5s, the stimulus reaches the minimum S-cone contrast and appears lime to the viewer.

photoreceptor stimulation. In the first three conditions, the discs flickered at 0.5 Hz, in either a monocular, binocular or dichoptic arrangement. In the dichoptic condition the non-target eye saw a flickering fixed contrast of 48%. In the remaining three conditions (the cross-frequency conditions) one eye's disc flickered at 0.4 Hz, and the other eye's disc flickered at 0.5 Hz. We also tested monocular responses at 0.4 Hz, as well as binocular (one eye sees each frequency at the target contrast) and dichoptic (target stimulus flickering at 0.5 Hz, mask contrast of 48% at 0.4 Hz in the other eye) arrangements. We counterbalanced presentation of the target stimulus across the left and right eyes.

For all experiments, sinusoidal contrast modulations were presented against the same background spectrum (matched between the eyes), which was used to achieve silent substitution in the three photoreceptor modulation experiments. The background spectra were defined by setting all channels to half maximum output for the brighter of the two devices (STLab 1, left eye) and then using the STLab 1/STLab 2 calibration ratio to find the equivalent settings for the companion device (STLab 2, right eye). The background spectrum illuminance was approximately 74 lux. The spectral power distributions and alpha-opic irradiances of the background spectra for both eyes are shown in Figures 1b-c.

3.3.1 Experiment 1: luminance

The experiment was conducted in a windowless room, in which the only source of light was the modified VR headset. The participants sat as close as possible to the VR headset, leaving enough space for the eye-tracker to record the eyes. The experiment was carried out in a single session of 45 minutes, divided into three blocks of 15 minutes each. In each block, there were a total of 60 trials lasting 15 seconds each (12s of stimulus presentation, followed by 3s of interstimulus interval). The participants were given no task other than look at the black fixation dot while trying to minimise their blinking during the presentation period.

In this experiment, the participants saw a disc of achromatic flickering light (average illuminance of approximately 74 lux), flickering between black and white, at the different contrast levels defined earlier. An example of one cycle of flickering for the luminance experiment is shown in Figure 2a. The spectral power distributions and alpha-opic irradiances relative to the background for the luminance experiment are shown in Figures 1d-e.

3.3.2 Experiment 2: melanopsin

The experiment used the same equipment set-up and the same experimental conditions as Experiment 5. The procedure was also the same. However, at the beginning of each block, participants habituated for 2 minutes to the background that would be present throughout the entire experiment. During this adaptation period, participants were asked to fixate on the same black fixation dot positioned in the middle of the stimulus and were told that they could blink normally. At the end of the adaptation period, the experiment started immediately and the participants followed the same instructions given in Experiment 1.

In this experiment, the participants experienced contrast modulations that targeted the melanopsin-containing intrinsically photosensitive Retinal Ganglion cells, while ignoring rods and nominally silencing the cones. Michelson contrast levels represented a percentage of the maximum melanopic contrast available, which was predetermined to be approximately 22 %. Under perfect silent substitution conditions, these modulations do not entail any changes in brightness or chromaticity: it is therefore very difficult to include an example to visualise the stimulus. However, silent substitution is never perfect, so participants reported small fluctuations in reddishness, greenishness and brightness due to open-field cone contrast artefacts. These fluctuations were especially present at higher contrasts. This can be observed in the alpha-opic irradiances relative to the background for the melanopsin experiment shown in Figure 1g, where a small activation of the S, L and M cones is observable. The spectral power distributions relative to the background for the melanopsin experiment is also shown in Figure 1f.

3.3.3 Experiment 3: L-M postreceptoral 'parvocellular' pathway

The experiment used the same equipment set-up and the same experimental conditions as Experiment 5. The procedure was the same as Experiment 6, including the presence of a 2-minute adaptation period at the beginning of each block. Additionally, before the start of the experiment, participants completed a luminance nulling perceptual calibration procedure in L-M cone space on an Iiyama VisionMaster^{TM} Pro 510 display (800 x 600 pixels, 60 Hz refresh rate). During the task, participants were presented with a disc flickering within the L-M cone space (between magenta and cyan). Using a trackball, participants adjusted the angle in cone space to find their subjective isoluminant point, which resulted in changing the flickering intensity of the stimulus until the amplitude of the flicker appeared to be minimised. The result was used to modify the requested contrasts during stimulus preparation so as to account for individual differences affecting perceived illuminance, principally the L:M cone ratio (Carroll et al., 2002; Hofer et al., 2005).

In this experiment, the participants experienced contrast modulations that targeted the L-M postreceptoral 'parvocellular' pathway while ignoring rods and nominally silencing S-cones and melanopsin. Michelson contrast levels represented a percentage of the maximum L-M contrast available for the background spectrum, which was determined in advance to be approximately 10 %. As shown in Figure 2b, participants experienced an isoluminant chromatic modulation between magenta (+L-M) and cyan (-L+M). The spectral power distributions and alpha-opic irradiances relative to the background for the L-M pathway experiment are shown in Figures 1h-i.

3.3.4 Experiment 4: S-(L+M) 'koniocelluar' pathway

The experiment used the same equipment set-up and the same experimental conditions as Experiment 5. The procedure was the same as Experiment 6, including the presence of a 2-minute adaptation period at the beginning of each block.

In this experiment, the participants experienced contrast modulations that targeted the S-(L+M) 'koniocelluar' pathway while ignoring rods and nominally silencing L/M cones and melanopsin. Michelson contrast levels represented a percentage of the maximum S-cone contrast available for the background spectrum, which was predetermined to be approximately 45 %. As shown in Figure 2c, participants experienced an isoluminant chromatic modulation between purple (+S-(L+M)) and lime (-S+(L+M)). The spectral power distributions and alpha-opic irradiances relative to the background for the S-(L+M) pathway experiment are shown in Figures 1j-k.

3.4 Data analysis

The pupillometry data were analysed using the same method we used in our previous study (Segala et al., 2023). The data were converted from mp4 videos to a csv text file using the Pupil Player software (Kassner et al., 2014), which estimated pupil diameter for each eye on each frame using a 3D model of the eyeball. The individual data were then loaded into R for analysis, where a ten-second waveform for each trial in each eye was extracted (excluding the first two seconds after stimulus onset). We interpolated across any dropped or missing frames to ensure regular and continuous sampling over time. The Fourier transform was calculated for each waveform, and all repetitions of each condition were pooled across eye and then averaged. Finally, data were averaged across all participants to obtain the group results. We used coherent averaging and at each stage we excluded data points with a Mahalanobis distance exceeding $D = 3$ from the complex-valued mean. The consensual response was also analysed (see Appendix 3 for more details and the results).

For all experiments, we used a bootstrapping procedure with 1000 iterations to estimate standard errors across participants. All analysis and figure construction was conducted using a single R-script, available online, making this study fully computationally reproducible: https://osf.io/gdvt4/.

3.5 Computational model and parameter estimation

To describe our data, we chose the same model described in our previous study (Segala et al., 2023). The model has the same general form as the first stage of the contrast gain control model proposed by Meese et al. (2006) and omits the second stage. For the previous model that we used (Segala et al., 2023), the exponent of the numerator had a fixed value of 2. Here, we allow this parameter (called p) to be free, in order to permit different shapes of contrast response function, e.g. saturating or super-saturating. The responses of the left eye and right eye channels are as follows:

$$Resp_L = \frac{L^p}{Z + L^q + wR^q}, \tag{1}$$

$$Resp_R = \frac{R^p}{Z + R^q + wL^q}, \tag{2}$$

where L and R are the contrast signals from the left and right eyes, p and q are exponents, Z is a saturation constant that shifts the contrast-response function laterally, and w is the weight of suppression from the other eye.

The responses from the two eyes are then summed binocularly:

$$Resp_B = R_{max}(Resp_L + Resp_R) + k, \tag{3}$$

where n is a noise parameter, and R_{max} scales the overall response amplitude.

We performed model fitting on the normalised amplitudes to account for amplitude differences between the experiments.

4 Results

4.1 Experiment 1

The results of the luminance experiment are summarised in Figure 3. The average Fourier spectrum is displayed in Figure 3a, and shows a strong response at the first harmonic frequency (0.5 Hz) and a weaker but still clear response at the second harmonic frequency (1 Hz). These results demonstrate that we can evoke measurable steady-state pupil responses at 0.5 Hz by stimulating the periphery of the retina. The group average waveform for binocular presentation is shown in Figure 3b. There is a substantial pupil constriction at stimulus onset, followed by very visible oscillations at the flicker frequency (0.5 Hz, see waveform at foot).

Figure 3d shows contrast response functions in response to stimuli flickering only at 0.5 Hz. The amplitude of the binocular condition (blue squares) is consistently greater than that of the monocular condition (red circles) across all target contrasts. A 2×5 repeated measures $ANOVA^2_{circ}$ (Baker, 2021) comparing these conditions revealed a significant main effect of target contrast ($F(8,220) = 80.82$, $p < 0.001$), a significant effect of condition ($F(2,220) = 52.88$, $p < 0.001$), and a significant interaction ($F(8,220) = 32.69$, $p < 0.001$). The dichoptic condition (green diamonds) begins at a much higher amplitude, owing to binocular combination of the target and high (48%) contrast mask, and then increases with increasing target contrast (main effect of target contrast: $F(8,184) = 38.89$, $p < 0.001$). Similar results can be observed at the second harmonic in Figure 3g (see Tables **??** and **??** for summary of statistical results).

In Figure 3e, we plot responses to monocular target stimuli flickering at 0.5 Hz, when the other eye viewed stimuli flickering at 0.4 Hz (the red monocular-only data are replotted from Figure 3d for comparison). When the 0.4 Hz component had the same contrast as the target (the binocular cross condition, shown in purple) responses were suppressed slightly across all target contrasts (interaction between contrast and condition: $F(8,220) = 29.51$, $p < 0.001$). When the 0.4 Hz component had a fixed contrast of 48 % (the dichoptic cross

condition, shown in yellow), responses were also suppressed slightly across the contrast range (interaction between contrast and condition: $F(8,220) = 27.52$, $p < 0.001$). The same pattern of results was generally observed at the second harmonic (Figure 3h, see Tables **??** and **??** for summary of statistical results).

Figure 3f shows responses at 0.4 Hz, for the same conditions, as well as for a condition in which a monocular stimulus flickered at 0.4 Hz (grey circles). Again there was evidence of weak suppression between the eyes, as the purple triangles fall below the grey circles (see Table **??** for summary of statistical results). The dichoptic cross condition also shows evidence of suppressive modulation with target contrast (see Table **??** for summary of statistical results). The same pattern is also observed at the second harmonic (Figure 3i, see Tables **??** and **??** for summary of statistical results).

Finally, we calculated the binocular to monocular ratio at the first and second harmonic frequencies. Figure 3c shows that these ratios are generally below 2 at both frequencies, suggesting that there is summation happening between the eyes but also interocular suppression, therefore suggesting that the signals between the eyes are combined non-linearly. At the highest contrast at the second harmonic, the ratio is close to 2, perhaps indicating that a more linear combination is happening for higher contrasts.

4.2 Experiment 2

The results of the melanopsin experiment are summarised in Figure 4. The average Fourier spectrum is displayed in Figure 4a, and also shows clear responses at both the first harmonic frequency (0.5 Hz) and the second harmonic frequency (1 Hz) of approximately equal amplitude. These results demonstrate that we can evoke measurable steady-state pupil responses at 0.5 Hz by selectively stimulating the melanopsin-containing retinal ganglion cells whilst ignoring rods and nominally silencing all three cone classes. The group average waveform for binocular presentation is shown in Figure 4b and shows a substantial pupil constriction at stimulus onset, followed by visible oscillations at approximately the flicker frequency (0.5 Hz, see waveform at foot).

Figure 4d shows contrast response functions for melanopsin-directed stimuli flickering at 0.5 Hz. The amplitude of the binocular condition (blue squares) is similar to that of the monocular condition (red circles) across all target contrasts (all error bars overlap, see Table **??** for summary of statistical results). At the second harmonic the binocular response is substantially greater than the monocular response at higher contrasts where the response is above baseline (Figure 4g, see Table **??** for summary of statistical results).

In Figure 4e, we again plot responses to monocular target stimuli flickering at 0.5 Hz, when the other eye viewed stimuli flickering at 0.4 Hz (here too, the red monocular-only data are replotted from Figure 4d for comparison). For the binocular cross condition (shown in purple), responses were slightly suppressed across all target contrasts (see Table **??** for summary of statistical results). For the dichoptic cross condition (shown in yellow), responses were also slightly suppressed across the contrast range (see Table **??** for summary of statistical results). This pattern is also observed at the second harmonic (Figure 4h, see Tables **??** and **??** for summary of statistical results).

Figure 4f shows responses at 0.4 Hz, for the same conditions, as well as for a condition in which a monocular stimulus flickered at 0.4 Hz (grey circles). These data are perhaps too noisy to interpret, though we note that the binocular cross data (purple triangles) are generally below the monocular data (grey circles), perhaps indicating suppression (see Table **??** for summary of statistical results). The same pattern is generally also observed at the second harmonic (Figure 4i, see Table **??** for summary of statistical results).

Finally, we calculated the binocular to monocular ratio at the first and second harmonic frequencies. Figure 4c shows that these ratios are around 1 at the first harmonic, suggesting that there is strong interocular suppression between the eyes, and binocular signal combination is therefore strongly non-linear.

4.3 Experiment 3

The results of the L-M pathway experiment are summarised in Figure 5. The average Fourier spectrum is displayed in Figure 5a, and shows clear responses at both the first harmonic frequency (0.5 Hz) and the

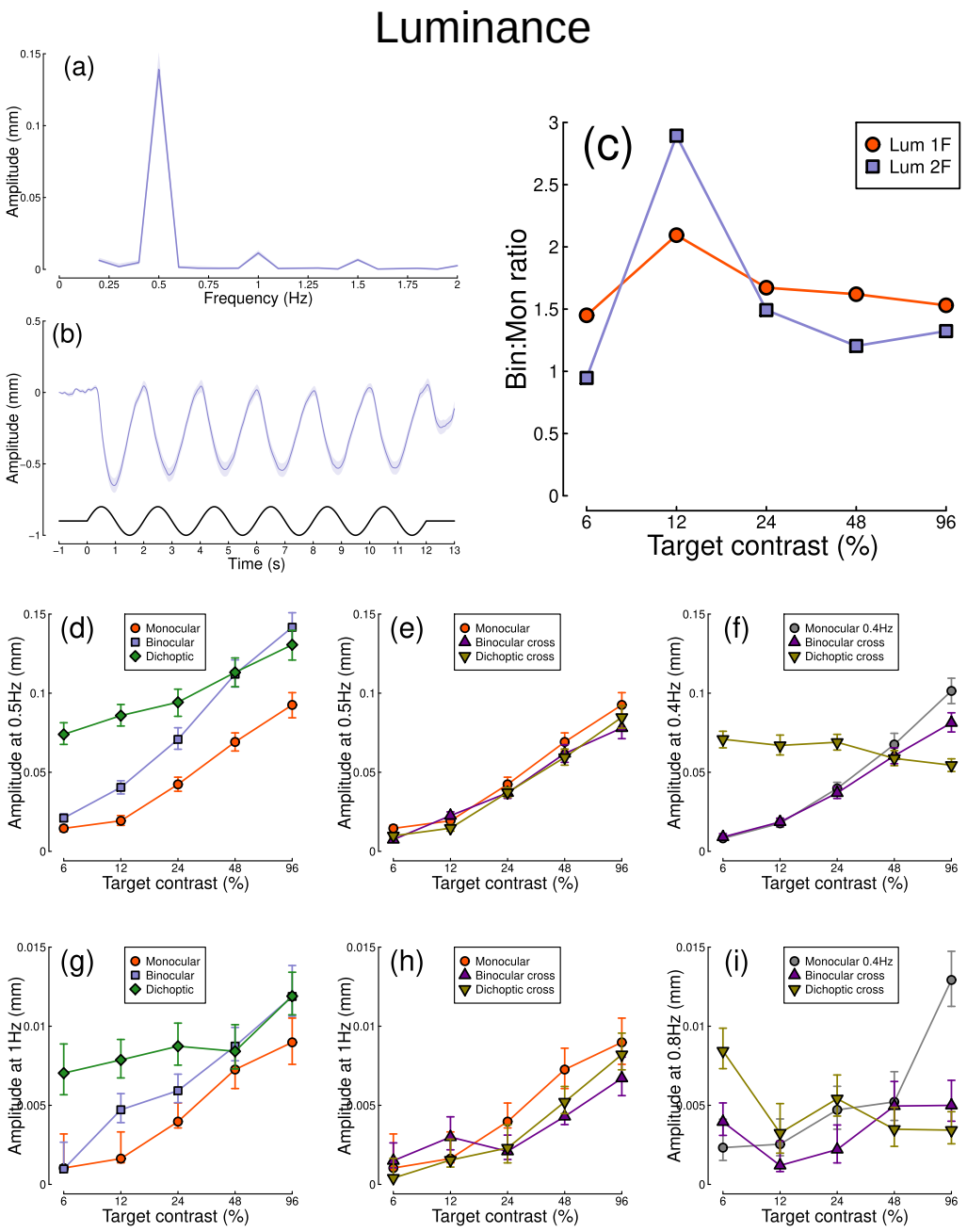

Figure 3: Summary of pupillometry results for the luminance experiment for N=12 participants. Panel (a) shows the average Fourier spectrum. Panel (b) shows a group average waveform for binocular presentation (low pass filtered at 5 Hz), with the driving signal plotted at the foot. Panel (c) shows the ratio of binocular to monocular response. The red circles show the ratios at the first harmonic (0.5 Hz) and the blue squares show the ratios at the second harmonic (1 Hz). Panels (d,e) show contrast response functions at 0.5 Hz for different conditions. Panel (f) shows contrast response functions at 0.4 Hz for three conditions. Panels (g-i) are in the same format but for the second harmonic responses. Shaded regions and error bars indicate bootstrapped standard errors.

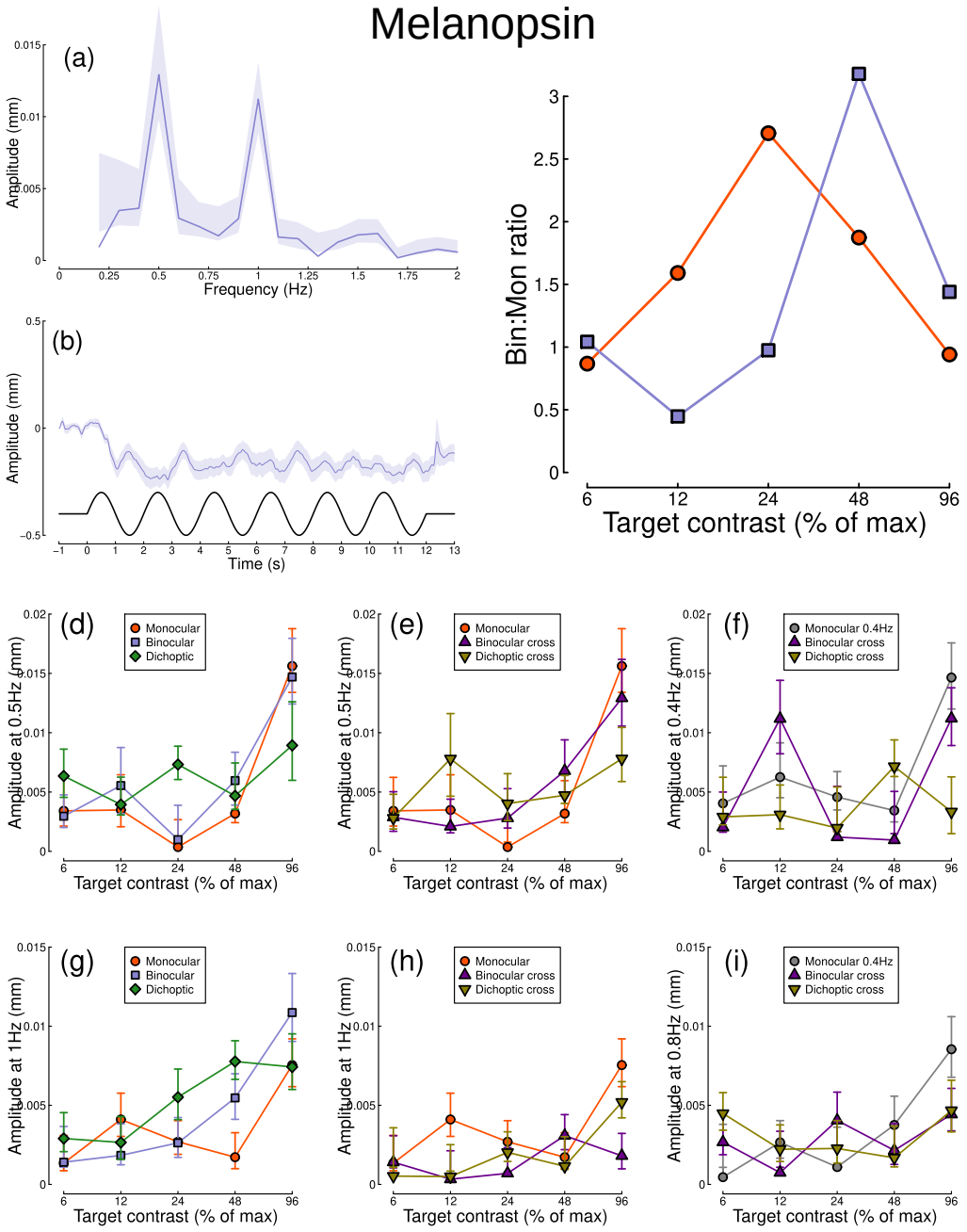

Figure 4: Summary of pupillometry results for the melanopsin experiment for N=12 participants. Panel (a) shows the average Fourier spectrum. Panel (b) shows a group average waveform for binocular presentation (low pass filtered at 5 Hz), with the driving signal plotted at the foot. Panel (c) shows the ratio of binocular to monocular response. The red circles show the ratios at the first harmonic (0.5 Hz) and the blue squares show the ratios at the second harmonic (1 Hz). Panels (d,e) show contrast response functions at 0.5 Hz for different conditions. Panel (f) shows contrast response functions at 0.4 Hz for three conditions. Panels (g-i) are in the same format but for the second harmonic responses. Shaded regions and error bars indicate bootstrapped standard errors.

second harmonic frequency (1 Hz) of approximately equal amplitude. These results demonstrate that we can evoke measurable steady-state pupil responses at 0.5 Hz by selectively stimulating the L-M postreceptoral 'parvocellular' pathway whilst ignoring rods and nominally silencing S-cones and melanopsin. The group average waveform for binocular presentation is shown in Figure 5b and, as observed in the previous experiments, there is a substantial pupil constriction at stimulus onset, followed by visible oscillations at the flicker frequency (0.5 Hz, see waveform at foot) and its second harmonic (i.e. there are two peaks in the data for every one peak in the driving waveform).

Figure 5d shows contrast response functions in response to stimuli flickering only at 0.5 Hz. The amplitude of the binocular condition (blue squares) is substantially smaller than that of the monocular condition (red circles) across the range of target contrasts, indicating a process of binocular suppression (see Table **??** for summary of statistical results). At the second harmonic, the pattern is reversed, with the binocular responses being larger than the monocular responses (Figure 5g, see Table **??** for summary of statistical results).

In Figure 5e, we plot responses to monocular target stimuli flickering at 0.5 Hz, when the other eye viewed stimuli flickering at 0.4 Hz (the red monocular-only data are replotted from Figure 5d for comparison). For the binocular cross (purple triangles) and dichoptic cross (yellow triangles) conditions, we again observed a very strong suppression of the responses across all target contrasts (see Tables **??** and **??** for summary of statistical results). This was not observed at the second harmonic (Figure 5h), where monocular and binocular responses appeared to be quite similar (see Tables **??** and **??** for summary of statistical results).

Figure 5f shows responses at 0.4 Hz, for the same conditions, as well as for a condition in which a monocular stimulus flickered at 0.4 Hz (grey circles). Again, strong suppression can be observed across the contrast range (see Table **??** for summary of statistical results). The dichoptic cross condition shows a clear modulation with target contrast, as we can see by the decrease of the response as the contrast increases (see Table **??** for summary of statistical results). The same pattern is also observed at the second harmonic (Figure 5i), though the suppression in the binocular cross condition is less extreme at the second harmonic (see Tables **??** and **??** for summary of statistical results).

Finally, we calculated the binocular to monocular ratio at the first and second harmonics. Figure 5c shows that these ratios are generally below 1 at the first harmonic, again indicating very strong interocular suppression, and suggesting that the combination of the signals between the eyes is strongly non-linear. At the second harmonic, the ratios are generally between 1 and 2, suggesting that suppression between the eyes is weaker, but overall the combination remains non-linear.

4.4 Experiment 4

The results of the S-(L+M) pathway experiment are summarised in Figure 6. The average Fourier spectrum is displayed in Figure 6a, and shows a clear response at both the first harmonic frequency (0.5 Hz) and a stronger response (by around 50%) at the second harmonic frequency (1 Hz). These results demonstrate that we can evoke measurable steady-state pupil responses at 0.5 Hz by selectively stimulating the S-(L+M) 'koniocelluar' pathway whilst ignoring rods and nominally silencing L/M cones and melanopsin. The group average waveform for binocular presentation is shown in Figure 6b. There is a substantial pupil constriction at stimulus onset, followed by very visible oscillations at the flicker frequency (0.5 Hz, see waveform at foot) and its second harmonic.

Figure 6d shows contrast response functions in response to stimuli flickering only at 0.5 Hz. For the first 3 target contrasts, response amplitudes increased monotonically with target contrast. At the higher contrasts, we observe a roll-over of the pupil response shown by the drop in the signals. This suggests that the S cones saturate at higher contrasts, and so are not able to drive larger pupil modulations. The amplitude of the binocular condition (blue squares) is consistently greater than that of the monocular condition (red circles) across the range of target contrasts (see Table **??** for summary of statistical results). At the second harmonic, we observe quite different results, with the binocular and monocular conditions having the same amplitudes across the contrast range (Figure 6g), and no evidence of saturation (see Table **??** for summary of statistical results).

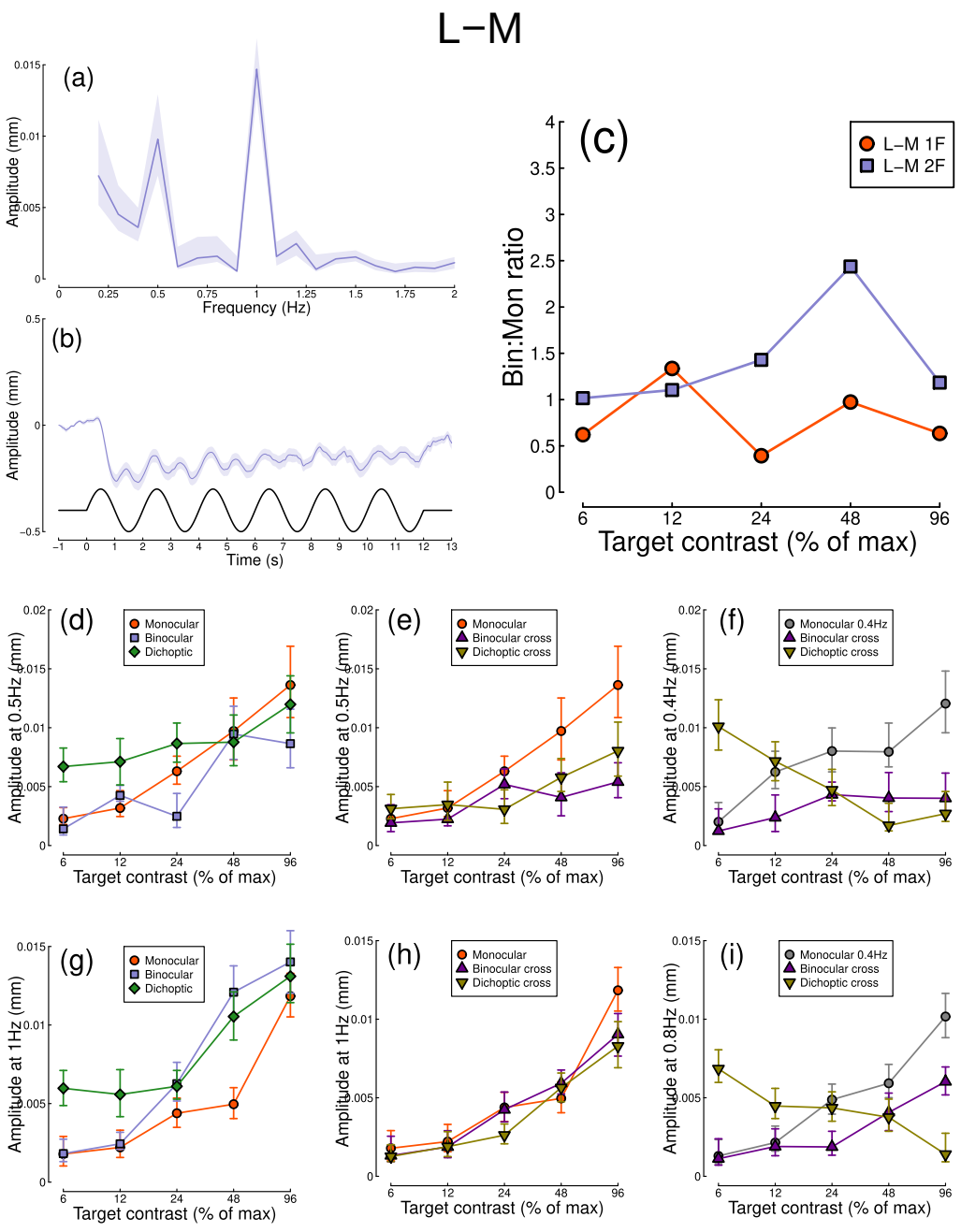

Figure 5: Summary of pupillometry results for the L-M pathway experiment for N=12 participants. Panel (a) shows the average Fourier spectrum. Panel (b) shows a group average waveform for binocular presentation (low pass filtered at 5 Hz), with the driving signal plotted at the foot. Panel (c) shows the ratio of binocular to monocular response. The red circles show the ratios at the first harmonic (0.5 Hz) and the blue squares show the ratios at the second harmonic (1 Hz). Panels (d,e) show contrast response functions at 0.5 Hz for different conditions. Panel (f) shows contrast response functions at 0.4 Hz for three conditions. Panels (g-i) are in the same format but for the second harmonic responses. Shaded regions and error bars indicate bootstrapped standard errors.

In Figure 6e, we plot responses to monocular target stimuli flickering at 0.5 Hz, when the other eye viewed stimuli flickering at 0.4 Hz (the red monocular data are replotted from Figure 6d for comparison). There was very little evidence of suppression in the binocular cross (purple triangles) or dichoptic cross (yellow triangles) conditions at the first harmonic (see Tables **??** and **??** for summary of statistical results). However at the second harmonic (Figure 6h), strong suppression was apparent at the higher target contrasts (see Tables **??** and **??** for summary of statistical results).

Figure 6f shows responses at 0.4 Hz, for the same conditions, as well as for a condition in which a monocular stimulus flickered at 0.4 Hz (grey circles). At this frequency there was some evidence of suppression at the higher target contrasts (purple triangles below grey circles, see Table **??** for summary of statistical results). At the second harmonic (Figure 6i), the binocular cross condition (purple triangles) shows a very strong suppression and the dichoptic cross condition shows a clear modulation with target contrast (yellow triangles), visible as a decrease of the response as the target contrast increases (see Tables **??** and **??** for summary of statistical results).

Finally, we calculated the binocular to monocular ratio at the first and second harmonics. Figure 6c shows that these ratios are generally between 1 and 2 at the first harmonic, indicating summation between the eyes with intermediate levels of interocular suppression. At the second harmonic, the ratios were around 1 for the three highest target contrasts, again consistent with strong interocular suppression.

4.5 Computational modelling

We fitted a computational model to the data from Experiments 1, 2, 3 and 4 using a hierarchical Bayesian approach. The model behaviour is displayed in Figure 7a-d for the first harmonic frequency and in Figure 7f-i for the second harmonic frequency. The empirical data is superimposed for comparison. In general, the model captures the key characteristics of the empirical data, with group-level parameter estimates provided in Tables 1 and 2 for the first and second harmonic frequencies respectively. We were particularly interested in comparing the weight of interocular suppression across data sets. We therefore plot the posterior distributions for this parameter for all four data sets (see Figure 7e for the distributions at the first harmonic and Figure 7j for the distributions at the second harmonic).

At the first harmonic, the key finding is that the luminance results (grey distribution) display a much smaller weight of interocular suppression than the other data sets. The melanopsin and S-(L+M) results (gold and blue distributions) display a similar weight of interocular suppression. The L-M results (red distribution) display the greatest weight of interocular suppression of all data sets. There is minimal overlap between the luminance distribution and the other three distributions. For the luminance, the distribution is meaningfully below a weight of 1, while it is well above a weight of 1 for the L-M results. The distributions of melanopsin and S-(L+M) are around a weight of 1. These results offer an explanation of the empirical data: the weaker suppression for the luminance experiment is consistent with the weaker suppression effects and the weaker dichoptic masking, while the stronger suppression for the L-M experiment is consistent with the stronger suppression observed at the first harmonic and the stronger dichoptic masking.

At the second harmonic, the key finding is that the S-(L+M) results display a greater weight of interocular suppression compared to the other data sets. On the other hand, the L-M results display the smallest weight of interocular suppression. The luminance and melanopsin results display weights of interocular suppression that are quite close to each other. For the L-M results, the distribution is meaningfully below a weight of 1, while it is well above a weight of 1 for the S-(L+M) results. The distributions of luminance and melanospin are around a weight of 1, with the former being slightly below and the latter being slightly above. These results offer an explanation of the empirical data: the weaker suppression for the L-M experiment is consistent with the weaker suppression effects and the weaker dichoptic masking observed at the second harmonic, while the stronger suppression for the S-(L+M) experiment is consistent with the stronger suppression observed at the second harmonic and the stronger dichoptic masking.

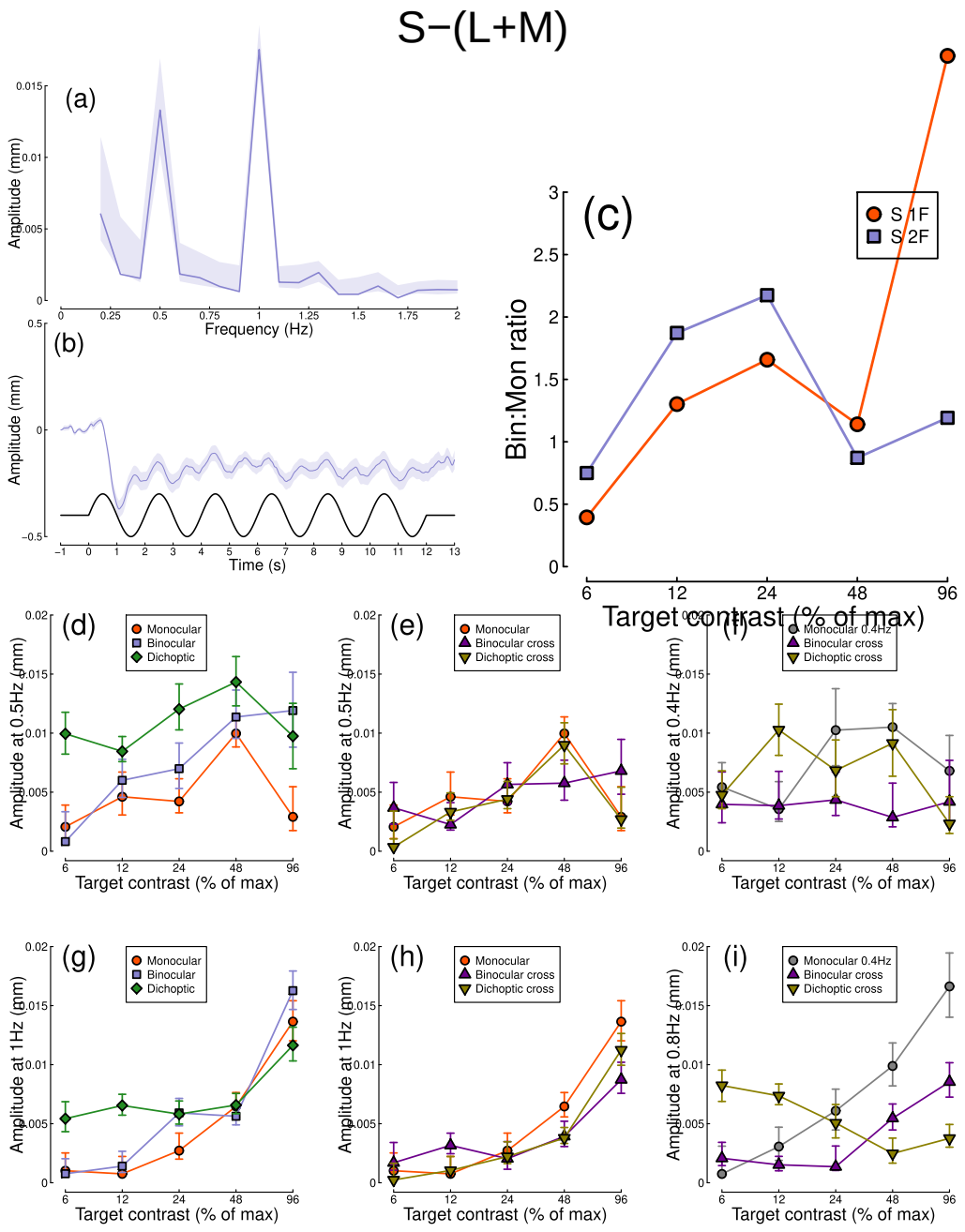

Figure 6: Summary of pupillometry results for the S-(L+M) pathway experiment for N=12 participants. Panel (a) shows the average Fourier spectrum. Panel (b) shows a group average waveform for binocular presentation (low pass filtered at 5 Hz), with the driving signal plotted at the foot. Panel (c) shows the ratio of binocular to monocular response. The red circles show the ratios at the first harmonic (0.5 Hz) and the blue squares show the ratios at the second harmonic (1 Hz). Panels (d,e) show contrast response functions at 0.5 Hz for different conditions. Panel (f) shows contrast response functions at 0.4 Hz for three conditions. Panels (g-i) are in the same format but for the second harmonic responses. Shaded regions and error bars indicate bootstrapped standard errors.

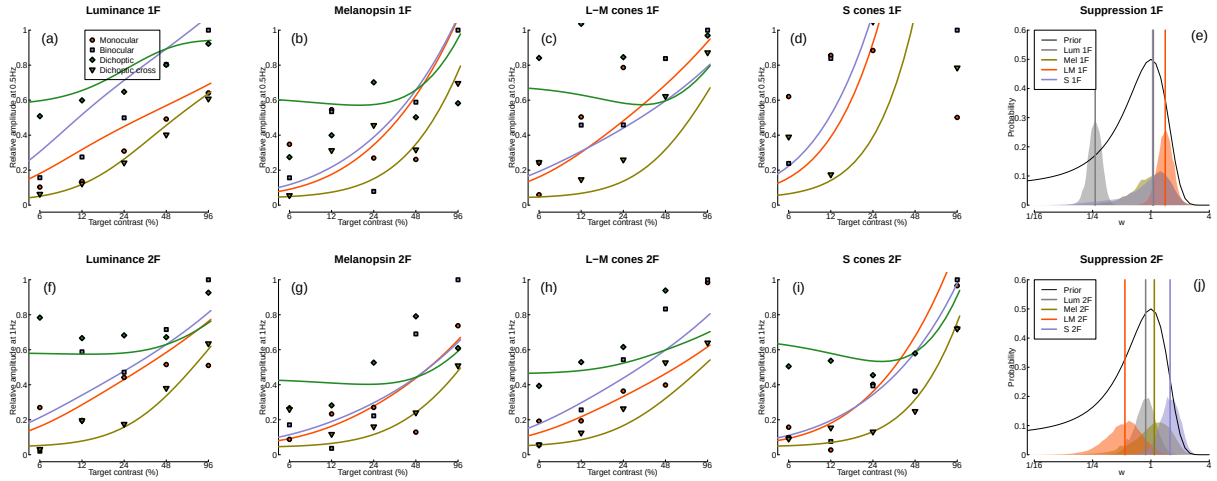

Figure 7: Summary of computational modelling. Panels (a-d) and (f-i) show empirical data from key conditions at the first and the second harmonic frequencies respectively. The data are replotted from earlier figures for the luminance experiment at the first (a) and the second (f) harmonic frequencies, the melanopsin experiment at the first (b) and the second (g) harmonic frequencies, the L-M pathway experiment at the first (c) and the second (h) harmonic frequencies, and the S-(L+M) pathway experiment at the first (d) and the second (i) harmonic frequencies. The curves show model behaviour generated using the median group-level parameter values. Panels (e) and (j) show the posterior probability distributions of the interocular suppression parameter for each of the four model fits at the first and the second harmonic frequencies respectively. In panel (e), the luminance distribution (grey) is centred about a substantially lower suppressive weight than for the other data types (note the logarithmic x-axis), while the L-M distribution (red) is centred about a higher suppressive weight than for the other data types. On the other hand, in panel (j), the L-M distribution is centred about a substantially lower suppressive weight than for the other data types, while it is the S-(L+M) distribution (blue) that is centred about a higher suppressive weight than for the other data types. The black curves show the (scaled) prior distribution for the weight parameter.

Table 1: Summary of median parameter values at the first harmonic frequency.

Experiment	Z	k	w	p	q	Rmax
Luminance 1F	21.15	0.02	0.27	1.91	1.66	0.21373
Melanopsin 1F	20.62	0.04	1.06	1.90	1.22	0.05084
L-M 1F	22.14	0.04	1.40	1.96	1.55	0.13861
S 1F	21.53	0.04	1.04	1.98	1.16	0.10229

Table 2: Summary of median parameter values at the second harmonic frequency.

Experiment	Z	k	w	p	q	Rmax
Luminance 2F	21.75	0.04	0.88	1.98	1.61	0.13592
Melanopsin 2F	20.67	0.04	1.08	1.91	1.36	0.05348
L-M 2F	21.70	0.04	0.54	1.95	1.55	0.09385
S 2F	21.42	0.04	1.57	1.97	1.24	0.04321

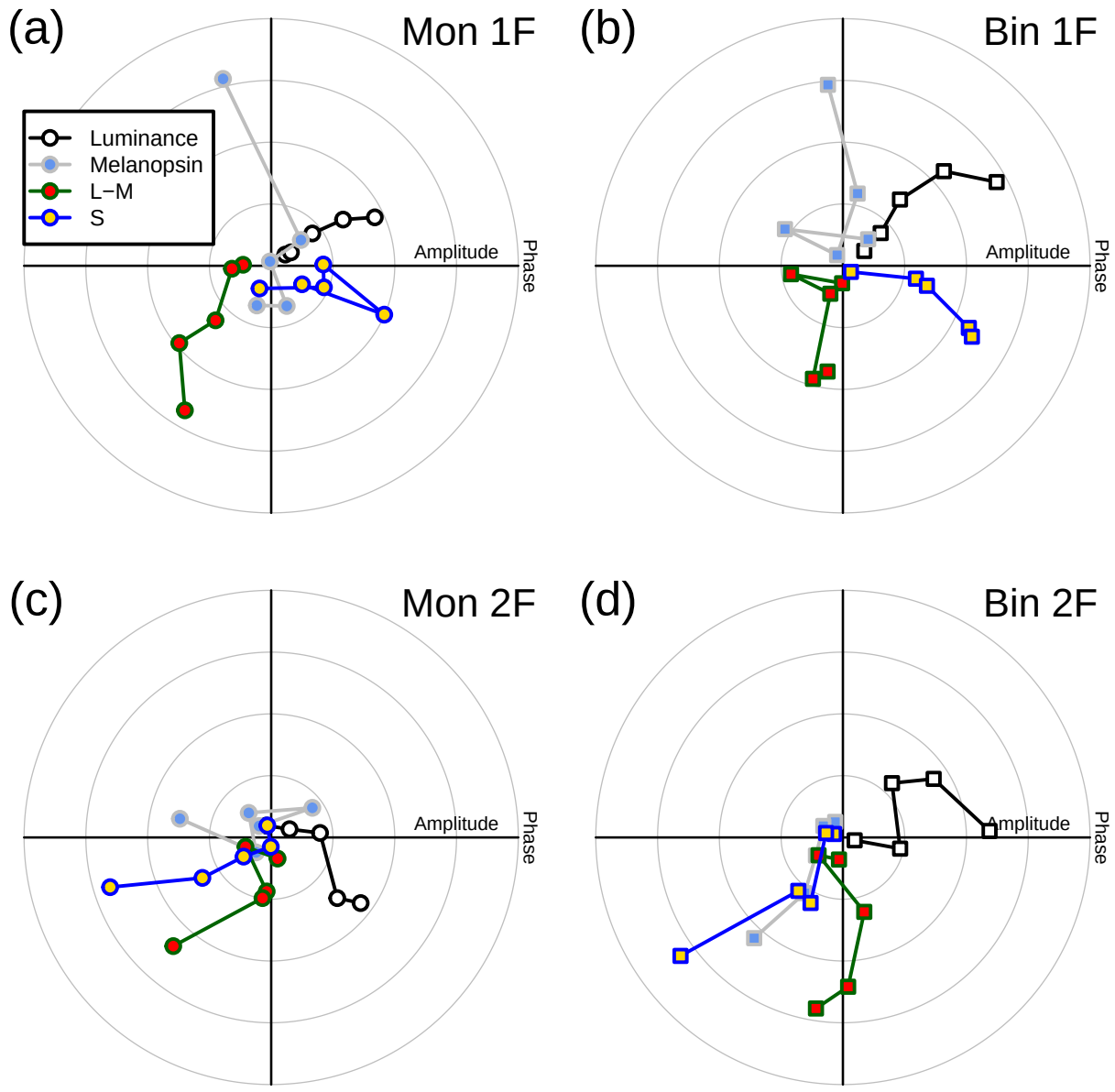

Figure 8: Pupil phase plots at the first and second harmonic frequencies for the luminance, melanopsin, L-M pathway and the S-(L+M) pathway experiments. Panel (a) shows the pupil response during monocular stimulation at the first harmonic frequency. Panel (b) shows the pupil response during binocular stimulation at the first harmonic frequency. Panel (c) shows the pupil response during monocular stimulation at the second harmonic frequency. Panel (d) shows the pupil response during binocular stimulation at the second harmonic frequency. In panels (a) and (b), the luminance amplitudes have been scaled down by a factor of 10 to be compared with the other experiments' results.

4.6 Phase analysis

In a previous study, Spitschan et al. (2014) analysed the phase of the pupil response and compared it between L+M-cone stimulation, S-cone stimulation, melanopsin stimulation and brightness stimulation. In their study, they found that, at a flicker frequency of 0.5 Hz, L+M and melanopsin responses were in phase, while brightness and S-cone responses were in anti-phase. Additionally, they found that, at the second harmonic frequency, S-cone and melanospin responses seem to be in phase with each other and in anti-phase to L+M-cone responses. We reproduced this analysis with our data and the results are summarised in Figure 8. At the first harmonic frequency, the amplitudes from the luminance experiment have been scaled down by a factor of 10 to make it possible to compare them directly with the results from the other experiments.

Figure 8a shows the results to monocular responses at the first harmonic frequency. The L-M pathway stimulation produces an anti-phase pupil response relative to luminance stimulation. The S-(L+M) pathway and luminance results are desynchronised in quadrature phase. This same pattern of results is also observable in Figure 8b, which summarises the results to binocular responses at the first harmonic frequency.

Figure 8c shows the results to monocular responses at the second harmonic frequency. Here, results are noisier compare to the first harmonic results, but a pattern is still observable. In general, it seems that melanopsin and S-(L+M) stimulations produce in-phase responses to each other, but produce anti-phase responses to luminance stimulation. On the other hand, L-M pathway responses seem to be desynchronised in quadrature phase from the the results of the other experiments. The same pattern of results is also observable in Figure 8d, which summarises the results to binocular responses at the second harmonic frequency.

5 Discussion

We used pupillometry and silent substitution to measure monocular and binocular responses of the pupils to flickering stimuli when stimulating specific photoreceptor pathways. In our luminance experiment, we found that peripheral stimulation of the retina can elicit a pupillary response and we were also able to record a response at the second harmonic, which was not seen when we stimulated the fovea (Segala et al., 2023). In all four experiments, we were able to record contrast response functions at both the first and the second harmonics. All experiments showed that binocular combination in the autonomic nervous system happens in a non-linear manner, with evidence of different magnitudes of interocular suppression depending on the photoreceptor pathway. This pattern of results was confirmed by a computational model, which allowed us to compare the weight of interocular suppression for each pathway. We found that, at the first harmonic frequency, the L-M pathway had a bigger suppression weight than the other pathways, while, at the second harmonic frequency, the S-(L+M) pathway had a bigger suppression weight. Finally, we looked at the pupil phases and observed different behaviours for the different pathways at the first and second harmonic frequencies. While the patterns differed between the first and second harmonics, within the same harmonic, whether the stimuli were presented monocularly or binocularly, the patterns were similar.

Our four experiments produced results that we were expecting based on our previous pupillometry findings (Segala et al., 2023): the signals between the 2 pupils are combined non-linearly regardless of which photoreceptor pathway is being stimulated and whether the fovea or the periphery of the retina is being stimulated. We also observed responses at both the first and the second harmonic frequencies, which were expected based on previous literature (Spitschan et al., 2014; Stark and Sherman, 1957; Verdon and Howarth, 1988). There was, however, one aspect of our results that we were surprised to observe: the amplitude of this second harmonic response in the different photoreceptor pathways. It is true that we had already observed second harmonic responses when stimulating the periphery of the retina with achromatic luminance modulations flickering at 2 Hz (see Figure **??**b), but the peak was very small when compared to the first harmonic peak, which is similar to what we observed in the luminance experiment here. On the other hand, in the melanopsin and L-M pathway experiments, the first and second harmonics are similar in amplitudes, and in the S-(L+M) pathway experiment, the peak of the second harmonic is even bigger than the peak of the first harmonic. One reason for why this might be happening may be because the driving signal is stronger when using a lower flicker frequency (indeed, pupillometry is more responsive to slow flicker frequencies of

less than 1 Hz, Spitschan et al., 2014) and when stimulating the periphery of the retina (we have a very clear waveform for the luminance experiment in Figure 3b). However, this explanation is not entirely satisfactory: we observed a second harmonic when stimulating the periphery using a higher flicker frequency and the pupil waveforms from the other three experiments are not as clear as the one from the luminance experiment. The presence of a second harmonic might indicate the existence of non-linearities that are not observable in the fovea: indeed, steady-state visual responses can contain activity beyond the first harmonic and these harmonics reflect non-linearities (e.g. squaring, exponentiation, rectification) in the visual response (Norcia et al., 2015). Additionally, it can be the case that, when these non-linearities are strong, then the higher harmonics can have equal or even higher peaks than the first harmonic. Here, we did observe strong non-linearities in our photoreceptor pathways, as reflected by the interocular suppression weights that were output by our computational model. For the S-(L+M) pathway specifically, it seems that the higher peak of the second harmonic is a behaviour intrinsic to S cones, as this was observed previously (Spitschan et al., 2014).

The pupil phases shown in Figure 8 give us more information about the pathways controlling the pupil response. The first thing that we notice is that the luminance and L-M pathway responses are in anti-phase. It is important to note that, for our L-M pathway stimulation, the stimulus flickered between magenta (first half of the cycle) and cyan (second half of the cycle), which means that the pupil was dilating during the magenta stimulation and then constricting during the cyan presentation. This seems to suggest that increments in magenta would correspond to decrements in brightness and increments in cyan would correspond to increments in brightness. It is possible that, if we had reversed the presentation cycle for the L-M pathway, the pupil response would have been in phase with the luminance responses. It has been recently shown that L-cone and melanopsin stimulation induce an opponent pupillary response to M- and S-cone stimulation (Murray et al., 2018; Woelders et al., 2018). Our melanopsin and S-(L+M) results show a similar behaviour both for monocular and binocular responses. The L-M pathways results are desynchronised approximately in quadrature phase from the melanopsin and S-(L+M) results. These results also seem to align with what was previously found: combining L and M responses should display results that are between the opponency shown by the isolated cone stimulation. Additionally, this could explain the very strong suppression that binocular (L-M) stimulation displays compared to the monocular stimulation: if L and M produce pupil responses that are in anti-phase with each other, then combining the two together should elicit smaller responses. Finally, since the results from our experiments are not in phase, it would suggest that the photoreceptors control the pupil diameter through different pathways.

6 Conclusions

We have demonstrated that binocular combination of temporal flickering light in the autonomic nervous system depends on the photoreceptor pathway. We were able to elicit pupil responses by stimulating only the periphery of the retina and we were able to record contrast response functions for all photoreceptor pathways. While all pathways showed non-linear combination, they showed a variation in how the signals are combined, particularly in the weight of interocular suppression.

7 Acknowledgements

Supported by Biotechnology and Biological Sciences Research Council grant BB/V007580/1 awarded to DHB and ARW.

References

Baker DH. 2021. Statistical analysis of periodic data in neuroscience. *Neurons, Behavior, Data analysis, and Theory* **5**. doi:10.51628/001c.27680

Baker DH, Lygo FA, Meese TS, Georgeson MA. 2018. Binocular summation revisited: Beyond $\sqrt{2}$. *Psychol Bull* **144**:1186–1199. doi:10.1037/bul0000163

Baker DH, Meese TS, Georgeson MA. 2007. Binocular interaction: Contrast matching and contrast discrimination are predicted by the same model. *Spat Vis* **20**:397–413. doi:10.1163/156856807781503622

Barrionuevo PA, Cao D. 2016. Luminance and chromatic signals interact differently with melanopsin activation to control the pupil light response. *Journal of Vision* **16(11)**:29. doi:10.1167/16.11.29

Barrionuevo PA, McAnany JJ, Zele AJ, Cao D. 2018. Non-linearities in the Rod and Cone Photoreceptor Inputs to the Afferent Pupil Light Response. *Frontiers in Neurology* **9**.

Barrionuevo PA, Nicandro N, McAnany JJ, Zele AJ, Gamlin P, Cao D. 2014. Assessing rod, cone, and melanopsin contributions to human pupil flicker responses. *Investigative Ophthalmology & Visual Science* **55**:719–27. doi:10.1167/iovs.13-13252

Campbell FW, Green DG. 1965. Monocular versus binocular visual acuity. *Nature* **208**:191–2. doi:10.1038/208191a0

Cao D, Nicandro N, Barrionuevo PA. 2015. A five-primary photostimulator suitable for studying intrinsically photosensitive retinal ganglion cell functions in humans. *Journal of Vision* **15**:27. doi:10.1167/15.1.27

Carroll J, Neitz J, Neitz M. 2002. Estimates of L:M cone ratio from ERG flicker photometry and genetics. *Journal of Vision* **2**:1. doi:10.1167/2.8.1

Dacey DM, Liao H-W, Peterson BB, Robinson FR, Smith VC, Pokorny J, Yau K-W, Gamlin PD. 2005. Melanopsin-expressing ganglion cells in primate retina signal colour and irradiance and project to the LGN. *Nature* **433**:749–754. doi:10.1038/nature03387

Dacey DM, Peterson BB, Robinson FR, Gamlin PD. 2003. Fireworks in the primate retina: In vitro photodynamics reveals diverse lgn-projecting ganglion cell types. *Neuron* **37**:15–27. doi:https://doi.org/10.1016/S0896-6273(02)01143-1

Ding J, Sperling G. 2006. A gain-control theory of binocular combination. *Proc Natl Acad Sci U S A* **103**:1141–6. doi:10.1073/pnas.0509629103

Gamlin PDR, McDougal DH, Pokorny J, Smith VC, Yau K-W, Dacey DM. 2007. Human and macaque pupil responses driven by melanopsin-containing retinal ganglion cells. *Vision Research* **47**:946–954. doi:10.1016/j.visres.2006.12.015

Hofer H, Carroll J, Neitz J, Neitz M, Williams DR. 2005. Organization of the human trichromatic cone mosaic. *The Journal of Neuroscience* **25**:9669–9679. doi:10.1523/jneurosci.2414-05.2005

Kassner M, Patera W, Bulling A. 2014. Pupil: An open source platform for pervasive eye tracking and mobile gaze-based interaction.Proceedings of the 2014 ACM International Joint Conference on Pervasive and Ubiquitous Computing: Adjunct Publication. ACM. doi:10.1145/2638728.2641695

Legge GE. 1984. Binocular contrast summation–ii. Quadratic summation. *Vision Res* **24**:385–94. doi:10.1016/0042-6989(84)90064-6

Lucas RJ, Hattar S, Takao M, Berson DM, Foster RG, Yau K-W. 2003. Diminished pupillary light reflex at high irradiances in melanopsin-knockout mice. *Science* **299**:245–247. doi:10.1126/science.1077293

Markwell EL, Feigl B, Zele AJ. 2010. Intrinsically photosensitive melanopsin retinal ganglion cell contributions to the pupillary light reflex and circadian rhythm. *Clinical and Experimental Optometry* **93**:137–149. doi:10.1111/j.1444-0938.2010.00479.x

Martin JT, Pinto J, Bulte D, Spitschan M. 2022. PyPlr: A versatile, integrated system of hardware and software for researching the human pupillary light reflex. *Behavior Research Methods* **54**:2720–2739. doi:10.3758/s13428-021-01759-3

Mathôt S. 2018. Pupillometry: Psychology, physiology, and function. *J Cogn* **1**:16. doi:10.5334/joc.18

McDougal DH, Gamlin PD. 2015. Autonomic control of the eye. *Comprehensive Physiology* **5**:439–473. doi:10.1002/cphy.c140014

McDougal DH, Gamlin PD. 2010. The influence of intrinsically-photosensitive retinal ganglion cells on the spectral sensitivity and response dynamics of the human pupillary light reflex. *Vision Research* **50**:72–87. doi:10.1016/j.visres.2009.10.012

McDougal DH, Gamlin PD. 2008. Pupillary control pathways.The Senses: A Comprehensive Reference. Elsevier. pp. 521–536.

Meese TS, Georgeson MA, Baker DH. 2006. Binocular contrast vision at and above threshold. *Journal of Vision* **6**:1224–43. doi:10.1167/6.11.7

Murray IJ, Kremers J, McKeefry D, Parry NRA. 2018. Paradoxical pupil responses to isolated M-cone increments. *Journal of the Optical Society of America A* **35**:B66–B71. doi:10.1364/JOSAA.35.000B66

Norcia AM, Appelbaum LG, Ales JM, Cottereau BR, Rossion B. 2015. The steady-state visual evoked potential in vision research: A review. *Journal of Vision* **15(6)**:4. doi:10.1167/15.6.4

Panda S, Sato TK, Castrucci AM, Rollag MD, DeGrip WJ, Hogenesch JB, Provencio I, Kay SA. 2002. Melanopsin (opn4) requirement for normal light-induced circadian phase shifting. *Science* **298**:2213–2216. doi:10.1126/science.1076848

Provencio I, Rodriguez IR, Jiang G, Hayes WP, Moreira EF, Rollag MD. 2000. A Novel Human Opsin in the Inner Retina. *Journal of Neuroscience* **20**:600–605. doi:10.1523/JNEUROSCI.20-02-00600.2000

Ruby NF, Brennan TJ, Xie X, Cao V, Franken P, Heller HC, O'Hara BF. 2002. Role of melanopsin in circadian responses to light. *Science* **298**:2211–2213. doi:10.1126/science.1076701

Segala FG, Bruno A, Martin JT, Aung MT, Wade AR, Baker DH. 2023. Different rules for binocular combination of luminance flicker in cortical and subcortical pathways. *eLife* **12**. doi:10.7554/elife.87048

Shapiro AG, Pokorny J, Smith VC. 1996. Conerod receptor spaces with illustrations that use CRT phosphor and light-emitting-diode spectra. *Journal of the Optical Society of America A* **13**:2319. doi:10.1364/josaa.13.002319

Spitschan M. 2019. Photoreceptor inputs to pupil control. *Journal of Vision* **19**:5. doi:10.1167/19.9.5

Spitschan M, Jain S, Brainard DH, Aguirre GK. 2014. Opponent melanopsin and s-cone signals in the human pupillary light response. *Proceedings of the National Academy of Sciences* **111**:15568–15572. doi:10.1073/pnas.1400942111

Spitschan M, Woelders T. 2018. The Method of Silent Substitution for Examining Melanopsin Contributions to Pupil Control. *Frontiers in Neurology* **9**.

Stark L, Sherman PM. 1957. A SERVOANALYTIC STUDY OF CONSENSUAL PUPIL REFLEX TO LIGHT. *Journal of Neurophysiology* **20**:17–26. doi:10.1152/jn.1957.20.1.17

Verdon W, Howarth PA. 1988. The pupil's response to short wavelength cone stimulation. *Vision research* **28**:1119–1128. doi:10.1016/0042-6989(88)90138-1

Wang C-A, Munoz DP. 2015. A circuit for pupil orienting responses: Implications for cognitive modulation of pupil size. *Curr Opin Neurobiol* **33**:134–40. doi:10.1016/j.conb.2015.03.018

Woelders T, Leenheers T, Gordijn MCM, Hut RA, Beersma DGM, Wams EJ. 2018. Melanopsin- and L-cone–induced pupil constriction is inhibited by S- and M-cones in humans. *Proceedings of the National Academy of Sciences* **115**:792–797. doi:10.1073/pnas.1716281115

Wyatt HJ, Musselman JF. 1981. Pupillary light reflex in humans: Evidence for an unbalanced pathway from nasal retina, and for signal cancellation in brainstem. *Vision Res* **21**:513–25. doi:10.1016/0042-6989(81)90097-3

Zele AJ, Feigl B, Adhikari P, Maynard ML, Cao D. 2018. Melanopsin photoreception contributes to human visual detection, temporal and colour processing. *Scientific Reports* **8**. doi:10.1038/s41598-018-22197-w